

Multiple object and integral field near-infrared spectroscopy using fibers

Roger Haynes¹, David Lee², Jeremy Allington-Smith, Robert Content, George Dodsworth, Ian Lewis², Ray Sharples, James Turner, John Webster, Christine Done, Reynier Peletier
Astronomical Instrumentation Group, University of Durham,
South Rd, Durham DH1 3LE, UK

Ian Parry
Institute of Astronomy, University of Cambridge,
Madingley Rd, Cambridge, CB3 0HA, UK

Scott Chapman
Dominion Astrophysical Observatory, Herzberg Institute of Astrophysics
5071 W. Saanich Rd, Victoria, BC, V8X 4M6, Canada

ABSTRACT

We describe a new system for multiple object spectroscopy and integral field spectroscopy at near-infrared wavelengths using optical fibers. Both modes of the SMIRFS instrument have been tested at the UK Infrared Telescope with the CGS4 infrared spectrograph. The modular system includes a common optical system to image the fiber slit onto the cold slit inside the CGS4 cryostat. The multiobject mode consists of 14 interchangeable fused silica or zirconium fluoride fibers each with a field of 4 arcsec. The integral field mode consists of 72 fused silica fibers coupled with a lenslet array to give a contiguous field of 6×4 arcsec with 0.6 arcsec sampling.

We describe the performance of both modes. For the multiobject mode, the feasibility and desirability of using fluoride fibers to extend the wavelength range into the K-band is discussed. For the integral field mode, the performance is compared with theoretical expectation with particular attention to the effect of Focal Ratio Degradation in the fibers.

These results demonstrate the feasibility of multiobject and integral field spectroscopy in the near-infrared using lenslet-coupled fiber systems. Although

¹E-mail: roger.haynes@durham.ac.uk

²Now at the Anglo-Australian Observatory

SMIRFS in an experimental system working with a spectrograph not designed for this purpose, the throughput and uniformity of response are good. SMIRFS points the way forward to systems with much larger numbers of elements.

Subject headings: Instrumentation, Integral field spectroscopy, Fibers, Near-infrared, Active galaxies

1. Introduction

SMIRFS is an instrument to explore new techniques for multiobject spectroscopy (MOS) and integral field spectroscopy (IFS) at near-infrared wavelength (1-2.5 μm). It was developed at low cost to provide the UK Infrared Telescope (UKIRT) with a simple capability in these areas and to develop the techniques needed to build larger-scale instruments for 4-m and 8-m telescopes. As such, the instrument was designed to a modest specification with the aim of building it quickly and obtaining useful results of use to other projects. The MOS and IFS modes of SMIRFS are referred to as SMIRFS-MOS and SMIRFS-IFS respectively.

In section 2, we describe the basic SMIRFS system consisting of the optical relay from the fiber slit to the cryogenic slit inside CGS4 and the multi-fiber system of the MOS mode. In Section 3, we describe the performance of this mode and present an example dataset obtained during commissioning. The IFS mode is described in Section 4. Its performance is presented in Section 5 which includes a comparison with theoretical expectations. In section 6, we give an example of a dataset obtained during commissioning which also serves to illustrate the operation of an integral field spectrograph. In Section 7, we state our conclusions and discuss the relevance of this work to other IFS systems under construction. We start by discussing the motivation for this work.

1.1. Multiobject spectroscopy in the infrared

To date, the technique of multiple object spectroscopy (MOS) has been almost exclusively employed at visible wavelengths. Although *Multi-slit* spectroscopy (e.g. LDSS-2, Allington-Smith et al. 1994, and GMOS, Murowinski et al. 1998) provides the best background subtraction because contiguous regions of sky within the same slit are sampled, this is bought at the expense of truncation of spectra near the edge of the field and some problems in addressing real target distributions. In contrast *multi-fiber* systems (e.g.

Autofib-2/WYFFOS, Parry et al. 1994, and 2dF, Taylor 1997) avoid these problems because the spectrum layout on the detector is independent of the field. However the accuracy of background subtraction is generally worse leading to limiting magnitudes which are 1-2 magnitudes brighter (see also Cuby & Mignoli 1994) and there are problems in addressing dense target distributions due to fiber collision restrictions.

The argument for Multiobject spectroscopy is just as strong in the infrared as in the visible, especially since the spectral energy distributions of field galaxies increasingly redshift to longer wavelengths so that the most useful spectral features appear in the near infrared. As an example of the surface densities to be encountered, the field galaxy population contains $\sim 10^4/\text{deg}^2$ at $K = 20$ which gives a multiplex gain of 10 in fields as small as 2 arcmin.

Extending multiobject techniques into the infrared is not straightforward. The difficulty of building a reconfigurable multiobject capability into a cryogenic instrument has so far ruled out signal/noise-optimized MOS at longer wavelengths ($> 1.8\mu\text{m}$) where it is necessary to encapsulate the optical system in a cryostat, although various systems are under development (e.g. EMIR for Gran Telescopio Canarias and the GIRMOS concept for GEMINI). However at shorter wavelengths, where the instrumental thermal background is not a problem ($1 - 1.8\mu\text{m}$), uncooled multi-fiber and multi-slit methods may be used (Herbst et al. 1995). Another issue is that current infrared instruments employ smaller detectors than in the visible. As we have seen, this poses some difficulties for multislit systems since they do not make optimum use of the detector surface whereas fibers can use this area more efficiently. This aspect makes it easier for multi-fiber systems to reach the high spectral resolutions required to reject the strong atmospheric OH emission lines which form most of the background in the J and H bands.

Consequently we decided to explore the use of a fiber-based MOS system in the near-IR up to the K-band. Since this wavelength range extends into the region where some drop in the performance of fused silica (FS) fibers may be expected ($> 2\mu\text{m}$), we decided to provide an alternative zirconium fluoride (ZF) fiber system. The use of ZF was also motivated by the possibility that fiber systems could be used in cryogenic instruments in which case fluoride fibers would definitely be required at the longer wavelengths which would then be accessible (up to $5\mu\text{m}$).

For reasons of cost, it was decided to use this prototype system with an existing infrared spectrograph: CGS4 (Ramsay-Howatt 1994) on UKIRT. This is a cryogenic instrument so a means had to be found to inject the reformatted light into it without rebuilding the cryostat. This was done using an optical relay between the uncooled fiber slit and the cold spectrograph slit which fits into the space normally occupied by CGS4's calibration

unit. The system was commissioned in June 1995 and December 1996. The first run was affected by very poor conditions. The second run had slightly better luck and incorporated an optional output mask to cut down thermal background from the fiber slit. Thereafter the system was adapted for integral field spectroscopy as described below.

1.2. Integral field spectroscopy in the infrared

Integral field spectroscopy (IFS) produces a spectrum from each part of a two-dimensional field (e.g. Bacon et al. 1995). In contrast, long-slit spectroscopy is limited to a one-dimensional field whose width is determined by the need to obtain good spectral resolution. IFS avoids this restriction by decoupling the slit width from the field shape by reformatting a rectangular field into a linear pseudo-slit. A further advantage is that precise target acquisition is not required since the object does not need to be carefully placed on a narrow slit. If desired, the acquisition can be checked by reconstructing a white-light image of the object by summing the two-dimensional spectrogram over wavelength. Even when observing unresolved objects in poor seeing, the system acts as an image slicer to eliminate slit losses.

The scientific motivation for integral field spectroscopy is summarized in Allington-Smith & Content (1998; hereafter AC) which also includes a discussion of sampling and background subtraction issues relevant to fiber-lenslet integral field spectrographs and describes the basic techniques. The fiber-lenslet technique used in SMIRFS ensures that the field is contiguous, with unit filling factor, whilst maximising throughput by optimal coupling with both the telescope and spectrograph.

Particular applications for IFS in the infrared include studies of the obscured nuclear regions of active galaxies; the optical-radio co-alignment of distant radio galaxies, and studies of shocks in star forming regions. An example given in this paper relates to active galaxies via imaging of diagnostic emission lines indicative of star formation and non-thermal emission. Many of the key diagnostic spectral features for star-forming regions appear in the infrared and familiar ionic emission lines in distant galaxies are redshifted into the infrared.

As discussed by AC, the fiber-lenslet technique provides significant benefits over lenslet-only systems (e.g. TIGER, Bacon *et al.* 1995) in terms of the efficiency with which the detector surface is addressed and the length of spectrum which can be obtained without overlaps between spatial elements. A lenslet-only system for UKIRT, where the available number of pixels was initially only 256×72 pixels, would involve significant compromise in

field and spectrum length. The fiber-lenslet approach also has advantages over fiber-only systems. Firstly, it provides much better coupling to the telescope and spectrograph. Without this, the very slow beam from the telescope (f/36) would result in very low throughput. Secondly, it provides unit filling factor whereas a fiber-only system wastes the light which strikes the cladding (and buffer, if present) between fiber cores. Therefore, the fiber-lenslet approach is the best for implementing an IFS capability on UKIRT. This approach has also been adopted by us for the Thousand-element integral field unit (TEIFU; Haynes et al. 1998), for the IFS capabilities of the VLT VIMOS (Lefevre et al. 1998) and for the GEMINI Multiobject Spectrographs (GMOS, Allington-Smith et al. 1997). Other systems using this technique are SPIRAL and COHSI (Kenworthy et al. 1998).

For these reasons, we decided to adapt the SMIRFS-MOS system to a fiber-lenslet integral field unit (IFU). This system, which re-uses the SMIRFS-MOS infrastructure, allows us to prove technology to be applied to TEIFU (now successfully commissioned) and the GMOS IFU.

The results in this paper refer to two observing runs with the SMIRFS-IFU system. One in June 1997, for initial technical commissioning was accompanied by very poor weather but the other, in March 1998, was more successful and allowed spectral-line mapping of active galaxies (Turner *et al.* in preparation, Chapman et al. in preparation). The first run used CGS4 with its short camera giving a sampling of one detector pixel per spatial element while the second run used the long camera with a sampling of 2 pixels per spatial element.

2. The SMIRFS-MOS system

The system is described in detail by Haynes (1995). Fig. 1 shows the layout of SMIRFS and its coupling to the telescope and CGS4. SMIRFS has been designed to mount onto the West Port of UKIRT, which is reserved for visiting instruments. There are essentially four parts to the system; the field plate unit, the guide fiber unit, the fiber bundle and the slit projection unit. Despite the name, the guide fiber unit is not usually used for guiding, but is mainly used for field acquisition and checking the field plate orientation.

2.1. Field plate unit

The field plate unit's function is to hold the field plate and thereby the input of the fiber bundle at the focal plane of the telescope. The focus of UKIRT is 196mm from the West face of the instrument support unit. The field plate contains pre-drilled holes which

correspond to the positions of the objects to be observed as well as extra holes to hold the acquisition fibers and dedicated sky fibers, if required. A different field plate is needed for each field. The fibers are fixed in small brass ferrules which are held in the field plate by a lock nut (Fig. 2). The field may be adjusted in rotation to correct for any misalignment between the field plate and the object field. The correction is performed once during the instrument set-up and does not normally require changing when a different field plate is installed. However, as a quick check, the guide fibers can be used to ensure the orientation is correct. The field plate unit also has a plate tensioner, that pulls on the centre of the field plate to distort it to approximate a spherical surface with a radius of 11.5m to ensure that all the fibers in the field are pointing correctly at the exit pupil of the telescope (the secondary mirror). Any error in the global fiber pointing can be corrected using the UKIRT dichroic mirror, which directs the infrared light to the required port, while letting the visible light through to the cross-head acquisition and guide camera. The available field is 4 arcmin across and the minimum fiber to fiber spacing is approximately 18 arcsec. Fibers may not be deployed within the central 14 arcsec, where the tensioner is attached.

2.2. Guide fiber unit

This unit consists of three fiber bundles. Each is a coherent bundle containing 7 fibers; one central fiber closely surrounded by a ring of 6. These are coupled to a camera via two magnifying lenses. This enables the operator to determine the centroid of up to three stars in the field and from that make corrections to the telescope pointing and field plate rotation. Originally a SCANCO intensified camera was used, but this was not sufficiently sensitive to the small amount of predominately red light that was reflected by the dichroic. It was later replaced with a CCD, which considerably improved the sensitivity. However, because the guide fiber unit uses the visible light that is reflected by the dichroic, a correction for atmospheric refraction may be required at large zenith distance. The diameter of a single guide fiber bundle corresponds to approximately 2.7 arcsec on the sky.

2.3. Multi-object fiber bundles

In MOS mode, SMIRFS has two fiber bundles each containing 14 fibers: a zirconium fluoride (ZF) system for use in the K band and an ultra-low OH fused silica (FS) system for the J and H bands. The throughput of different fiber type is shown in Fig 3. A small CaF_2 lenslet (Fig. 2) is used at the input and output of each fiber to couple the telescope beam (f/36) into the fiber at f/5 and then back to f/36 at the output for coupling to the

spectrograph. This reduces losses due to focal ratio degradation¹ (FRD) within the fibers. The input lenslet (diameter 3mm, focal length 7.6mm) re-images the telescope exit pupil onto the face of the fiber core (200 μ m diameter). The pupil size was chosen to almost completely fill the fiber core so as to reduce the amount of light contamination from the sky around the secondary mirror, which is un baffled at UKIRT. This also reduces thermal contamination from any telescope structure around the top end.

At the bundle output, the fibers are re-formatted into a long slit. Each fiber is coupled to the CGS4 spectrograph via another lenslet which is identical to the lenslet at the fiber input. The centre to centre spacing along the fiber slit is 4mm, which corresponds to 6.2 arcsec at the detector. This corresponds to 5 pixels with the short camera (focal length 150mm) and 10 with the long camera (focal length 300mm). The fiber output spacing was constrained primarily by the number of detector pixels that are available along the CGS4 slit and the desire to maximize the multiplex gain. SMIRFS was originally designed for use with the 256 \times 256 array and the short camera which results in only 72 pixels along the slit.

The lenslets limit the aperture viewed by the fiber to 4.5 arcsec. However, this can be reduced to 2 arcsec in good seeing conditions by the use of a field stop mounted on the front of the fiber ferrule. This is not advisable for K band spectroscopy as the stop will contribute significantly to the thermal background as it is not cooled.

The thermal background is kept to a minimum by using the CGS4 spectrograph's cooled Lyot stop to mask out any contamination from beam angles faster than $f/36$ and by imaging the fiber slit onto the cooled CGS4 long slit. After the first telescope run it was found that there was a significant amount of thermal background from the slit material between the fibers. The slit was then modified by placing a reflective mask just in front of the fiber slit. This contained 14 holes to allow the light from the fibers to pass through and was positioned at such an angle that only light which had originated in CGS4 was reflected back into it, which, being cooled, produces very little thermal background. Each hole acts as a field stop limiting the effective aperture to ~ 2.5 arcsec on the sky. However, the aperture is slightly blurred by FRD effects so some light will come from outside a diameter of 2.5 arcsec. The slit mask considerably reduced the thermal contamination from the slit material, and is discussed in the next section.

¹A non-conservation of Etendue which results in the output beam being faster than the input beam. It is an equivalent to an increase in entropy so should be avoided.

2.4. Slit projection unit

As the spectrograph is a cryogenic instrument it was impractical to replace the CGS4 long slit with the SMIRFS fiber slit. It was therefore necessary to project the image of the fiber slit through the cryostat window into CGS4. This is achieved using a spherical re-imaging mirror and a plane fold mirror. In order to imitate the flat slit of CGS4 it was necessary to curve the fiber slit to match the field curvature of the re-imaging mirror, thus producing an image magnification of unity. Both mirrors are mounted on a tip/tilt and translation stage to facilitate alignment of the fiber slit with the CGS4 optical axis.

3. SMIRFS-MOS performance

3.1. Efficiency

The first commissioning run took place in June 1995 (Haynes 1995, Haynes et al. 1995) using the short CGS4 camera and a 75 lines/mm grating. The run was badly affected by poor weather but the provisional results obtained led to a number of modifications, the most significant of which was the reflective mask for the ZF fiber bundle to reduce the thermal background in the K band.

The second run in December 1996 used the same spectrograph configuration as June 95. The weather was partially clear but unsuitable for photometric studies much of the time. During the remainder of the time, photometric variation was around 10% which limits the accuracy of the results presented. The purpose of the run was primarily to observe a number of K and M giant star in both open and globular clusters to establish a new method of metal abundance determination for cool stellar population and demonstrate the potential of SMIRFS and future infrared fiber systems.

A summary of the throughput performance of SMIRFS (CGS4 short camera and grating) is given in Table 1. This gives the efficiency of the SMIRFS alone, obtained from a comparison of the count rates with the SMIRFS-MOS installed and with it removed from CGS4 so that light enters the spectrograph directly through the slit.

The predicted values are estimates that take into account the average fiber transmission, reflection losses and optical alignment errors (see Haynes 1995 for further details). The FS fiber throughput agrees reasonable well with the predictions, especially in the H and K bands. The results for the ZF without the output mask bundle agree well with the predictions, but the results with the output mask installed are significantly lower. This may be due to vignetting by the mask, resulting from mis-alignment of the star on the fiber

input or vignetting by the CGS4 slit due to flexure (Kerr 1997).

The problem of flexure within CGS4 became more apparent during the SMIRFS IFU run discussed later. The fiber to fiber throughput variations are $\sim 10\%$ RMS (Fig. 4) and are dominated by errors in the alignment between the fiber inputs and the telescope pupil.

3.2. Image quality

The PSF of the system can be demonstrated from a comparison of an observation of a standard star with SMIRFS and by CGS4 alone using just a long slit (Fig. 5). Gaussian fits to the cores of the two profiles indicate $\sigma = 0.56$ and 0.64 pixels with and without SMIRFS respectively. Although this comparison does not take the seeing into account, it suggests that any degradation in spatial resolution by SMIRFS is small and that the wings of the distribution arise from within CGS4. This is not surprising since the radial distribution of light in the object should be preserved at the slit (because the fibers preserve the radial *angular* distribution of light), except for the effect of FRD. This suggests that FRD is not a significant problem. No obvious sign of truncation of the PSF due to the effect of the output mask is seen: the results are similar for the FS (unmasked) and ZF fibers (masked and unmasked).

3.3. Background removal

Although background subtraction, by e.g. beam-switching, will remove the background whether it arises from the instrument or the sky, the signal/noise is degraded by the photon noise from the background. Therefore it is important to minimize the source of background before it is recorded by the detector.

Although the poor conditions during the June 1995 run mean that it is not possible to make a quantitative comparison of the thermal background of SMIRFS with and without the output slit mask, a large reduction in the inter-fiber background for the K band was noted after the output mask was installed. When observing sky the signal from the inter-fiber area was less than the signal from the fiber across the whole of the K band whereas previously it was often higher. This is shown in Fig. 6 where the background count rate using the mask is plotted separately as the component from the fiber alone and from the inter-fiber gap. This excludes thermal background from the sky and telescope but includes any contribution from CGS4 since this could not be determined independently. For this reason the count rates are upper limits.

Before the output mask was installed, a comparison of data taken with and without SMIRFS showed that the thermal background between 2.2 and 2.5 μm was only ~ 3 times larger for SMIRFS than for CGS4 alone (Haynes 1995). Although we were unable to make a direct comparison after the mask was installed, we believe that the thermal background due to SMIRFS is significantly less than implied by the figures given above.

3.4. Examples of data

An example of the K band spectra from giant stars in a globular cluster field (NGC1904) is shown in Figs 7 and 8. Beam switching was used for sky subtraction, by means of a telescope nod, typically a few arcmin. The observing sequence was 12 exposures of 5 seconds with 2×2 sampling (4 minutes) in a series of on-off-off-on target positions. This was repeated 8 times to give a total on-target time of 64 minutes. The data has been wavelength calibrated with an Argon arc spectrum and then co-added. The typical NaI (2.204 μm) and weak CaI (2.258 μm) absorption, plus the CO bands at redder wavelength (Terndrup et al. 1991), are visible in the brightest of the objects. It is also encouraging that the fibers dedicated to sky indicate negligible sky subtraction errors. Table 2 contains a list of the objects, their magnitudes and broad-band colors in the top-bottom order in which they appear in Fig. 8.

4. The SMIRFS-IFS system

4.1. The principle of fiber-lenslet IFS systems

As described in Section 1.2, fiber-lenslet systems have advantages over both lenslet-only systems in terms of the efficiency with which the detector surface is used — leading to an increase in field of view for fixed sampling increment and detector format — and fiber-only systems in terms of efficiency and filling factor. The basic principle of the SMIRFS integral field unit (IFU) is shown in Fig. 9. An image of the sky is formed on the input lenslet array. This forms images of the telescope pupil on the cores of a matching array of fibers bonded to the unfigured side of the lenslet array. This performs two functions: firstly, the beam is made faster to reduce the effect of FRD (Section 2.3) and, secondly, all the light falling on the lenslet aperture is captured by the fiber leading to almost unit filling factor. It is very important that as much light as possible is directed into the fibers which requires careful control of positional errors between the lenslets and fibers. In a visible-light system the fiber cores could be oversized but this is not desirable in the infrared because it would

inject background light into the fibers. For this reason, the core size is well-matched to the telescope pupil. The fibers are reformatted into a pseudoslit which consists of a line of fibers bonded to a linear lenslet array. The output of each fiber is a scrambled image of the telescope pupil from which each lenslet forms a scrambled sky image while ensuring that the beam is well-matched to CGS4. The resulting line of images, which forms the actual pseudoslit, is then re-imaged onto the cold slit of CGS4 inside its cryostat in the same way as for the SMIRFS-MOS system.

Overlaps in the distribution of light between elements at the slit are permissible since this only results in a small degradation in spatial resolution in the slit direction (AC). But this requires that the mapping between the IFU input and output is such that objects which are adjacent on the sky are also adjacent at the slit. This condition is satisfied by the ‘snakewise’ mapping shown in Fig 10. To completely avoid overlaps would require a separation between the IFU outputs at the slit which would drastically reduce the number of spatial elements.

4.2. Description of the SMIRFS IFU

Full details can be found in Lee (1998). Table 3 provides a summary. The SMIRFS-IFU reformats a rectangular field of 6×4 arcsec onto the CGS4 slit. The field is sampled by 72 hexagonal elements of size 0.6 arcsec. A spectrum is produced from each element when dispersed by the spectrograph. The number of elements is determined by the slit length of CGS4. With the short camera, the sampling is 1 pixel/element, but 2 pixels/element if the long camera is used. The sampling scale was a balance between the desire to exploit good images available from the UKIRT tip-tilt secondary mirror and the need to cover a useful field of view, given the limited number of elements.

The system consists of a field plate unit which supports the input of the IFU at the telescope focal plane, the lensed fiber bundle and a slit projection unit that projects the IFU slit onto the CGS4 slit. The slit projection unit and field plate unit are part of the SMIRFS-MOS system. The system is uncooled since it is not possible to package the system within the CGS4 cryostat. For this reason, the system is optimized for the J and H bands, although some useful performance may be expected in the K band, albeit with some instrumental thermal background.

The field plate unit is mounted on a port of the Instrument Selection Unit at 90° azimuth to CGS4. When the dichroic is correctly positioned, infrared light from the sky is focussed onto the IFU input. Visible light continues through the dichroic and forms an

image on the cross-head camera which is used for acquisition and guidance.

The IFU input (Fig 10) consists of a microlens array which forms images of the telescope pupil on the fiber cores. The fibers (Table 4) are individually located in an array of microtubes (Fig. 11) to an accuracy of $7\mu\text{m}$ RMS. The overall RMS positional accuracy of the fiber cores with respect to the lenslets is $\leq 10\mu\text{m}$. This includes the non-concentricity of the fibers with respect to their outer diameter, the non-concentricity of the fibers with the microtubes and positional errors within the microlens array. A small chimney baffle reduces background contamination by preventing light from entering the fibers at large angles.

The fibers are grouped together in a conduit and led into the slit plate unit which is installed in place of the CGS4 calibration unit. The fibers are terminated at 12 *slit blocks* where the fibers are interfaced to linear microlens arrays to form the slit (Figs 12 and 13). The fibers were found to be positioned with an accuracy of $7.5\mu\text{m}$ RMS with the largest error being $23\mu\text{m}$. The fibers are attached to the flat end of the output microlens arrays (Fig. 14) which focus parallel rays emerging from the fibers to form a scrambled image of the sky within each of the subapertures at the location of the IFU slit. Each block is angled to ensure that the principal arrays arrive at CGS4 with the same angle as when beam-fed directly from the telescope.

The lenslet arrays were made by *Adaptive Optics Associates* and consist of convex lens surfaces replicated in epoxy on a fused silica substrate. Tests of the lenslets show good position accuracy within the array. Measurements of the PSF for both input and output arrays show a well-concentrated diffraction-limited core with extended wings (see Section 6.4.3 of Lee 1998 and Lee et al. 1998). The wings are believed to arise from small defects in the lens surfaces. Table 5 shows detailed predictions from a numerical model of the IFU efficiency using realistic models of the loss mechanisms based on measurements of the lenslet PSF and FRD taking diffraction into account and assuming that the scattering losses are proportional to the inverse square of wavelength (Nussbaum et al. 1997). This suggests that the dominant loss mechanism ($\sim 20\%$) is the mismatch between the fiber core and the imperfect pupil image produced at the fiber input. Recall that the pupil image was not undersized with respect to the fiber core because of the need to baffle light from outside the telescope exit pupil.

The throughputs of the epoxy used in the lenslet fabrication and the adhesive used for bonding to the fiber array are shown in Fig 15. Note that the lenslet arrays are not antireflection coated as the epoxy surface is not suitable for this process.

The fiber slit is reimaged onto the cold CGS4 slit using a spherical mirror and a flat

mirror mounted in the slit plate unit. By adjustments of these mirrors the magnification, offset and focus of the image of the IFU slit can be adjusted. CGS4 is used with a 2-pixel wide slit to cut down scattered light while not vignetting the IFU slit, whose elements each project onto a circle of diameter ~ 1 pixel.

In the construction, much care was devoted to the following critical areas:

1. Random lenslet-fiber misalignments. As discussed above, these are such that the RMS misalignment at input and output is no greater than $10\mu\text{m}$ RMS.
2. The fibers were polished as complete units within their respective holders to ensure a flat surface for mating to the lenslet arrays. An additional advantage of using lenslets is that any residual roughness in the fiber ends is filled in by the optical adhesive.
3. FRD. This was measured for the completed fiber bundle before the lenslet arrays were bonded and found to be such that a parallel beam at the input produced a cone of light corresponding to $\sim f/10$ at the output. This was achieved by careful adjustment of the fiber bundle conduit to relieve stress on the fibers.
4. Alignment of the lenslets with the fibers. This is a complex procedure which eliminates not only global shifts and rotation of the lenslet arrays with respect to the fibers but also the non-telecentricity of the telescope feed to the spectrograph to ensure correct pupil alignment. It was estimated that the angular misalignment about the optical axis was $< 0.3^\circ$ and the positional accuracy was $< 20\mu\text{m}$. Any global shift is compensated for during alignment at the telescope.

5. On-telescope performance

5.1. Alignment and flexure

At the telescope, the following alignments were carried out.

1. The IFU input was aligned so that the telescope exit pupil (the secondary mirror) was aligned with the fiber cores. This was done by back-projecting light from the fiber slit onto the telescope secondary mirror and adjusting the angle of the dichroic which diverts infrared light to the IFU.
2. The relay-optics were adjusted to give unit magnification and to eliminate angular misalignment between the fiber slit and cold slit. This was achieved by masking the

input lenslet array to produce a diagnostic pattern at the slit which was recorded by the science detector.

3. Flexure test were done to examine the structural stability of the IFU plus spectrograph. Some flexure was found amounting to a maximum of 1.1 pixels (Lee 1998). However this is believed to be caused by flexure within CGS4 since it is similar to recent measurements made on CGS4 alone (Kerr 1997).

5.2. Efficiency

The efficiency of the IFU was measured by comparing observations of standard stars taken with CGS4 alone and with the IFU plus CGS4 with a wide slit. The results are summarized in Table 5. This excludes the efficiency of CGS4, its detector, the telescope and atmosphere. Considering that this instrument is a retrofit to a spectrograph not designed for IFS, the relative throughput of $\sim 50\%$ is very good.

One uncertainty in this estimate is whether all the light from the star passed through the CGS4 slit when used without the IFU. This can be estimated from the spatial profile along the slit on the assumption that the profile in the perpendicular direction is the same. Unfortunately, it is not known if the extended wings of the spatial profile (see Fig. 5 for an example of an observation with CGS4 alone) arise from within the spectrograph (as suggested in Section 3.2) or before the slit. If the latter is true, the measured throughput values should be multiplied by 0.92. The theoretical efficiency prediction in the table includes all known sources of error including misalignment errors, FRD and lenslet scattering based on laboratory measurements.

5.3. Uniformity and background subtraction

An important aspect of fiber-lenslet IFUs is the uniformity of response over the extent of the field. Large variations in response have the potential to complicate data reduction and, even if they can be removed by flatfield calibration, will compromise the final signal/noise since results will be degraded by regions of low response. The uniformity of response is indicated in Fig. 16. There is significant variation with an RMS of 16% of the mean. This includes one fiber which was broken during manufacture and others where it was noted during manufacture that the fiber was significantly displaced from its correct position. Nevertheless, these variation can be removed using standard flatfield calibration to within the limits imposed by photon statistics (Lee 1998).

Since there is no field dedicated to background subtraction, because of the limited slit length of CGS4, the technique of beam-switching is used. This is the same technique routinely used for CGS4 longslit observations. The telescope is nodded between two positions on (A) and off (B) the target in the sequence ABBA which is repeated as often as required. If the exposure time per pointing is short enough the background will be accurately subtracted. The temporal power spectrum of background variations is a matter of some controversy and varies from night to night and site to site. Our data show background residuals consistent with the results expected for CGS4 alone. There is no reason to believe that the IFU is more susceptible to these problems than any other instrument using this technique. However, ideally the IFU should be equipped with a dedicated field for background subtraction so that background estimates can be obtained contemporaneously (AC).

5.4. Point spread function

Here we assess the point-spread function (PSF) due to single elements of the IFU as a test of the quality of the system. The actual PSF observed will depend on the seeing and the method of reducing the IFS data. It is important to distinguish the PSF measured in the *slit direction* and *dispersion direction* in the raw data from the *spatial* PSF measured in orthogonal directions in the reconstructed image of the field.

The PSF in the spectral direction was measured from observations of wavelength calibration sources. CGS4 has the option to dither the detector (moving the detector by sub-pixel amounts before re-combining into a single frame in software) which allows the PSF to be properly sampled. In the J-band, the recorded line FWHM was equivalent to using a 1.1-pixel wide slit. In the H-band the effective IFU slit width is 1.2 pixels. With the IFU, CGS4 is normally used with a 2-pixel wide slit to ensure that a large fraction of the light from the fiber slit passes into the spectrograph. In fact, observations with CGS4 with a 1-pixel wide slit gives FWHM= 1.15 ± 0.05 pixels which implies that use of the IFU does not degrade the spectral resolution. However, the spectral PSF does vary slightly from fiber to fiber in the sense that fibers with lower efficiency also produce broader profiles (by up to $\sim 20\%$). This may be because these fibers are affected by FRD for which light exits from the fiber core at larger angles than usual leading to a broadened PSF at the slit. This would produce both a broadened image on the detector and lower efficiency since light emerging from the fibers at large angles would be vignetted by the output microlenses.

Checks were also done to see if the images at the slit were displaced in the dispersion direction. This would complicate the interpretation of data because of overlaps between

images from adjacent fibers. This test indicates that while there was a small non-linear distortion term amounting to ~ 0.1 pixel from a linear fit, no fiber output was displaced by more than $80\mu\text{m}$ from the average position.

Finally it should be noted that the reconstructed image profiles are slightly broadened in the direction which corresponds to the slit direction because of the overlap of images at the slit. As discussed by AC, this results in a small degradation in spatial resolution in this direction but has little effect on the spatial resolution in the orthogonal. For the image shown in Fig. 20, which is mostly unresolved, the cores of the profiles are well-fit by gaussian functions with FWHM of 1.32 and 1.07 arcsec in the direction parallel and perpendicular to the slit respectively. This is consistent with a seeing FWHM of 1.0 arcsec which indicates that the object is undersampled. AC provided a methodology for estimating this broadening effect which is due to the overlaps between images at the slit and depends on the amount of FRD present. However, in practice, the broadening is likely to be dominated by uncompensated flexure (Section 5.1) which will also produce a preferential broadening in the slit direction, and which may be present at the level of a few tenths of an arcsec.

6. Observing with the IFU

Here we outline the procedures required for data reduction. We present the example of an observation of NGC4151 to illustrate the operational techniques required.

6.1. Data reduction

Dispersed images from the CGS4 spectrograph are captured by a 256×256 InSb detector. With the SMIRFS-IFU and long camera, a 256×178 subsection is read out non-destructively, effectively providing bias-subtracted images by comparing consecutive exposures. A single integration, limited in duration mainly by background variability, may consist of a number of exposures which are individually short enough to avoid saturation. These are automatically combined by control software to form the raw data available to the user.

The raw integrations are typically obscured by high levels of dark current in $\sim 4\%$ of pixels, but this is removed effectively by sky subtraction. For extragalactic work, noise is sky dominated (or dominated by dark current for some pixels). To achieve full spectral resolution, critical sampling of the slit width requires a shift of the detector by half a pixel

between integrations and interlacing pairs of images. In practice extra steps are used, covering two pixel widths, to reduce the impact of dead pixels.

The process of reconstructing three-dimensional (x, y, λ) maps of target objects from the raw CGS4 integrations can be broken into the following main steps:

1. For each object integration (Fig. 17), the corresponding sky integration is subtracted, removing background and dark current.
2. The integration is divided by a detector flat image, taken before installing the IFU.
3. Integrations taken at different detector positions are combined into a single observation (Fig. 18), using an algorithm which also excludes pixels with anomalous values by comparison with a running median.
4. The spectra are extracted from each observation. Since the output of each element is not individually resolved along the slit, the positions must be calculated from known offsets.
5. Extracted spectra are divided by the extracted *fiber flatfield* exposure, to correct for variations in element transmission.
6. The spectra are reformatted into an (x, y, λ) datacube (Fig. 19), using the known mapping between position in the field and position in the slit, and by fitting a bidimensional surface to the spatial points at each wavelength increment.
7. If spatial mosaicing has been used to increase the field of view, the observations of each mosaic cycle are combined using information derived from the telescope offsets or by centroiding on known features. The individual datacubes are interpolated onto an output datacube with sub-pixel accuracy (Fig. 20).
8. Finally, the datacube is analysed to provide the required astrophysical diagnostics such as the distribution of continuum light in specified bands, the radial velocity field derived from the shift in any of the spectral features present and emission line ratios.

This procedure has been coded into a series of IRAF tasks specially written for the purpose.

6.2. Observations of NGC4151

At infrared wavelengths it is possible to view the centres of active galaxies from which visible light is obscured by dust in the torus. A fiber-lenslet IFU gives two-dimensional spectroscopy with the full wavelength resolution and coverage of a conventional long slit. Thus accurate spectral line strengths and corresponding velocities can be mapped across an object from a single observation revealing any association with structures seen in broad-band images or radio observations. Such an ability to form connections between spectral and physical features has proved crucial in identifying line excitation mechanisms.

Understanding excitation is important for studying kinematics as well as energy transfer. Previous work (Hutchings et al. 1998, Gallimore *et al.* 1997) suggests that the optical narrow line regions (NLR) of Seyfert galaxies are driven by photoionization via a cone of radiation from the active nucleus. This scenario is compatible with gravitationally dominated dynamics in those regions, indicated also by measurements of velocity dispersion (Nelson & Whittle 1996). However, emission may also occur through shock excitation (Genzelet al. 1995), in which case corresponding velocity measurements cannot be used to constrain the overall galactic gas kinematics. The strongest near-infrared emission lines in active galaxies are two forbidden [Fe II] transitions (1.26 and $1.64\mu\text{m}$), produced in regions where hydrogen is partially ionized. Usually the transition between ionized and neutral hydrogen is very sharply defined, so there has been recent speculation as to the how the partially ionized regions may arise (Veilleux et al. 1997). Proposed mechanisms involve X-ray photoionization of optically thick narrow line clouds, or shocks from either supernova remnants in starbursts or the interaction of a radio jet with the interstellar medium.

The $1.257\mu\text{m}$ [Fe II] line in the J-band falls close to $\text{Pa}\beta$, at $1.28\mu\text{m}$; the ratio $[\text{Fe II}]/\text{Pa}\beta$ has been found to be greater where emission is due to shock excitation than where photoionization dominates (Simpson et al. 1996), so helps to separate X-ray illumination from radio jet induced shocks. The two emission lines can be observed simultaneously with the 150 lines/mm grating in CGS4 (albeit without much bare continuum for reference), and, being so close together, provide a combined indicator which is relatively insensitive to reddening.

As an example, we show preliminary results for NGC4151, one of a number of nearby Seyfert galaxies observed in March 1998. To search for extended line emission over a field much larger than the nucleus, we constructed a mosaic using offsets from the nucleus. This also resulted in better sampling depending on location within the field.

Fig. 20 shows data from 51 IFU observations in 7 overlapping fields of view. The observations were combined into a single $78 \times 106 \times 257$ element datacube as described in

Section 6.1. In this galaxy, the axes of the radio jet and optical extended narrow line region are separated in the sky by ~ 25 degrees. The intention was to trace the infrared NLR emission far enough away from the nucleus to see whether it follows the jet or the optical NLR, thereby constraining the mechanism of excitation.

Fig. 21 shows maps in the central region of [FeII] and Pa β narrow-line intensity. There is clear evidence that the [FeII] emission is extended along the optical ENLR axis and marginal evidence for an extension in the narrow-component of Pa β . Further details, will be presented by Turner et al. (in preparation).

7. Conclusions

We have demonstrated the potential of lenslet-coupled fibers in the non-thermal regime for integral field and multiple-object spectroscopy in the near infrared. The integral field system gives significant advantages over fiber-only and lenslet-only systems. We have demonstrated good performance and utility for astronomy even with a low-cost prototype system retrofitted to an existing spectrograph.

The multiobject mode of SMIRFS provides a significant multiplex advantage in observing efficiency over the longslit spectrographs currently used at these wavelengths and points the way forward for infrared multi-fiber systems. Fiber systems offer efficient matching of the detector to a large field of view and make it easier to reach the high spectral resolution necessary to reject atmospheric OH emission lines.

At present, the number of fibers is limited only by the length of the CGS4 long slit and the small field of UKIRT (4 arcmin). With a dedicated spectrograph the multiplex advantage could be much increased. With more work the thermal emission from the fiber slit could be reduced further without impacting the throughput, leading to an increase in signal/noise at longer wavelengths.

With the integral field mode of SMIRFS, we have demonstrated how to use fiber-lenslet systems for efficient integral field spectroscopy in the near infrared. This work has also given us invaluable information for the construction of the recently-commissioned *Thousand Element Integral Field Unit* (TEIFU) and the fiber-lenslet system for the *GEMINI Multiobject Spectrographs* (GMOS). Both will include dedicated fields for background subtraction. Although these systems will initially operate at visible wavelengths, they can be extended with minor modification to work in the near-infrared.

With fused silica fibers, we can operate efficiently within the wavelength range where

instrumental thermal background is not a problem ($< 1.8\mu\text{m}$). However, work at longer wavelengths will require a cooled system. Although fibers are not the preferred technology for fully cryogenic operation, where image slicers (such as the *Advanced Image Slicer*; Content 1997) are likely to give much better performance, fibers may still be usable in cooled systems where full cryogenic temperatures are not required.

It may even be possible to use fibers in fully cryogenic environments since preliminary results from tests on cold fibers suggest that both the FRD and, more unexpectedly, the flexibility, are satisfactory for some types of unmounted fiber under such conditions (Haynes & Lee, private communication). The retention of flexibility is of considerable importance to *multiple* integral field spectroscopy since it suggests that fiber-lenslet systems could be deployable under cold conditions (see also Thatte et al. 1998).

We thank Simon Morris for his help with the scientific programme. We are indebted to the staff of the Joint Astronomy Centre in Hawaii for help with the integration of SMIRFS with UKIRT and CGS4, particularly Tom Kerr and Tom Geballe. We also thank Adaptive Optics Associates (Carol Dwyer and Brian McNeil) for their work on the microlens arrays. This work was largely supported by a grant from the UK Particle Physics and Astronomy Research Council.

REFERENCES

- Allington-Smith, J., Breare, J., Ellis, R., Gellatly, D., Glazebrook, K., Jorden, P., MacLean, J., Oates, A.P., Shaw, G., Tanvir, N., Taylor, K., Taylor, P., Webster, J. & Worswick, S.P. 1994, *PASP* 106, 983-991
- Allington-Smith, J., Content, R., Haynes, R., & Lewis, I. 1997, *Proc. SPIE*, 2871, 1284-1294
- Allington-Smith, J., & Content, R. 1998, *PASP*, 110, 1216-1234
- Bacon, R., Adam, G., Baranne, A., Courtes, G., Dubet, D., Dubois, J. P., Emsellem, E., Ferruit, P., Georgelin, Y., Monnet, G., Pecontal, E., Rousset, A. & Say, F. 1995, *A&A*, Suppl. 113, 347B
- Content, R. 1997, *Proc. SPIE*, 2871, 1295-1305
- Cuby, J-G. & Mignoli, M. 1994, *Proc. SPIE*, 2198, 98-109
- Gallimore, J., Baum, S., & O’Dea, C. 1997, *Nature*, 388, 852
- Genzel, R., Weitzel, L., Tacconi-Garman, L., Blietz, M., Cameron, M., Krabbe, A., Lutz, D., Sternberg, A. 1995, *ApJ*, 444, 129

- Haynes, R. 1995, PhD thesis, University of Durham
- Haynes, R., Sharples, R. & Ennico, K. 1995, *Spectrum*, 7, 4
- Haynes, R., Doel, P., Content, R., Allington-Smith, J., & Lee, D. 1998, *Proc. SPIE*, 3355, 788-809
- Herbst, T., Pitz, E., & Reuther, C. 1995, in ‘Tridimensional Optical Spectroscopic Methods in Astrophysics’, ASP Conf. Ser. 71, p221, eds G. Comte & M. Marcelin
- Hutchings, J., Baum, S., Weistrop, D., Nelson, C., Kaiser, M., & Gelderman, R. 1998, *AJ*, 116, 634
- Kenworthy, M., Parry, I. & Taylor, K. 1998, *Proc. SPIE*, 3355, 926
- Kerr, T. 1997, CGS4 Handbook on the *Wordwide Web*
<http://www.jach.hawaii.edu/UKIRT.new/instruments/cgs4/handbook.html>.
- Lee, D., Allington-Smith, R., Content, R. & Haynes, R. 1998, *Proc. SPIE*, 3355, 810-820.
- Lee, D. PhD thesis, University of Durham 1998
- LeFevre, O., Vettolani., G., Saisse, M., Maccagni, D., Mancini, D., Picat, J. & Mellier, Y. 1998, *Proc. SPIE*, 3355, 8
- Murowinski, R., Bond. R., Crampton, D., Davidge, T., Fletcher, J., Leckie, B., Morbey, C., Roberts., S., Saddlemyer, J., Sebesta, J., Stilburn, J., Szeto. K., Allington-Smith, J., Content, R., Davies, R., Dodsworth, G., Haynes, R., Robinson, D., Robertson, D., Webster, J., Lee, D., Beard, S., Dickinson, C., Kelly, D., Bennet, R., Ellis, M., Williams, P. 1998, *Proc. SPIE*, 3355, 188-194.
- Nelson, C., & Whittle, M. 1996, *ApJ*, 465, 96
- Nussbaum, P., Volkel, R., Herzing, H., Eisner, M. & Haselbeck S. 1997, *Pure & Applied Optics*, 6, 617
- Parry, I., Lewis, I., Sharples, R., Dodsworth, G., Webster, J., Gellatly, D., Jones, L. & Watson, F. 1994, *Proc. SPIE*, 2198, 125
- Ramsay-Howatt S. 1994, *Proc. SPIE*, 2198, 467
- Simpson C., Forbes, D., Baker, A. & Ward, M. 1996, *MNRAS*, 283, 777
- Taylor, K. 1997, *Proc. SPIE*, 2871, 145-149
- Terndrup, D., Frogel, J. & Whitford, A. 1991, *ApJ*, 378, 742
- Thatte, N., Tecza, M., Eisenhauer, F., Mengel, S., Krabbe, A., Pak, S., Genzel, R., Bonaccini, D., Emsellem, E., Rigaut, F., Delabre, B., & Monnet, G. 1998, *Proc. SPIE*, 3353, 704-715

Veilleux, S., Goodrich, R. & Hill, G. 1997, ApJ, 477, 631

Table 1: Summary of SMIRFS efficiency in MOS mode

	J	H	K	Reference fiber
Fused silica	0.51	0.62	0.57	7
Prediction	0.65	0.65	0.53	
Zirconium fluoride (with output mask)	0.39	0.41	0.42	4
Zirconium fluoride (with no output mask)	0.56	0.65	0.75	4
Prediction	0.55	0.62	0.69	

Table 2: Stars observed in NGC1904 (brightest to faintest)

Fiber	star	V	B-V
8	A41	12.94	1.41
12	A51	13.33	1.39
7	A45	13.84	1.18
13	A53	13.02	1.71
3	A50	13.49	1.76
14	A55	14.93	1.04
5	A42	15.28	0.97
2	A52	14.68	1.06
9	A54	15.78	0.86
6	A47	15.27	0.67
11	A44	16.12	0.82
4	A49	16.07	0.83
10	SKY		
1	SKY		

Table 3: Summary of SMIRFS-IFU

<i>Requirements:</i>	
Number of spatial elements	72
Spatial sampling	0.6 arcsec
Field of view	6×4 arcsec
Wavelength range	1–1.8 μ m optimized 1–2.5 μ m total
<i>Design parameters:</i>	
Focal ratio from telescope	f/36
Input lenslet pitch	412 μ m
Input focal length (air)	5.35mm
Fiber core diameter	150 μ m
Fiber input focal ratio	F/13
Fiber output focal ratio	F/8
Output lenslet pitch	793 μ m
Focal ratio into CGS4	F/40

Table 4: Details of SMIRFS-IFU fibers

Core material	Fused silica low OH
Core diameter	$151 \pm 2\mu\text{m}$
Numerical aperture	0.22 ± 0.02
Core-cladding ratio	1.1
Buffer material	Polyimide
Buffer diameter	$195 \pm 3\mu\text{m}$
Transmission range	$0.38 - 2.5\mu\text{m}$
Fiber length	1.2m

Table 5: Summary of SMIRFS-IFU efficiency in the J and H bands.

Loss mechanism	J	H
Misalignment with secondary mirror	0.99	0.99
Fiber transmission	0.998	0.997
Lenslet fresnel loss	0.921	0.923
Lenslet + adhesive transmission	0.996	0.968
Input fiber–lenslet geometrical loss	0.811	0.795
Output fiber–lenslet geometrical loss	0.969	0.964
IFU-spectrograph pupil geometrical loss	0.940	0.948
Slit projection mirrors	0.910	0.929
Theoretical IFU efficiency	0.61	0.60
Measured IFU efficiency	0.50	0.46

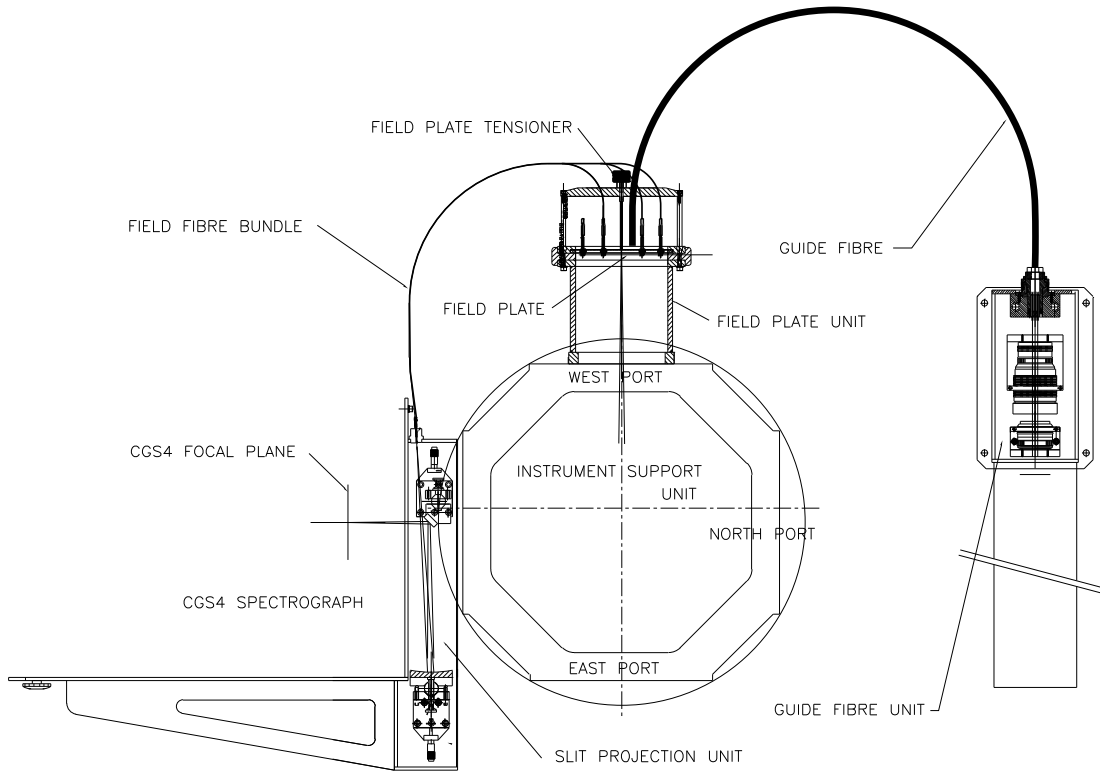


Fig. 1.— A plan view schematic of the layout of SMIRFS in multi-object mode

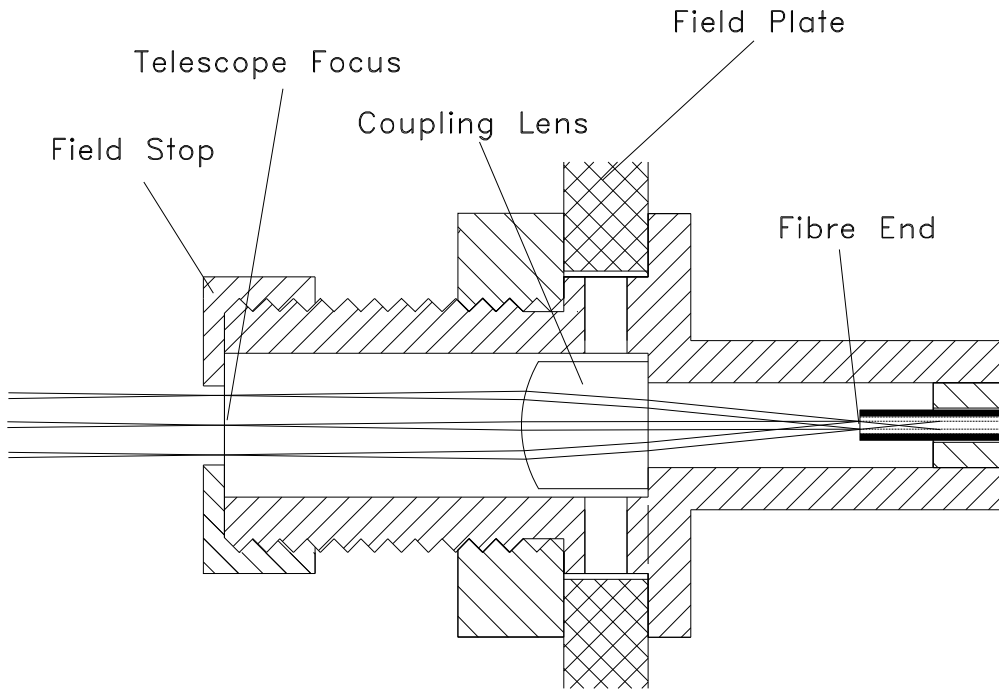


Fig. 2.— Schematic of a MOS-mode fiber ferrule showing the lenslet, fiber and optional field stop.

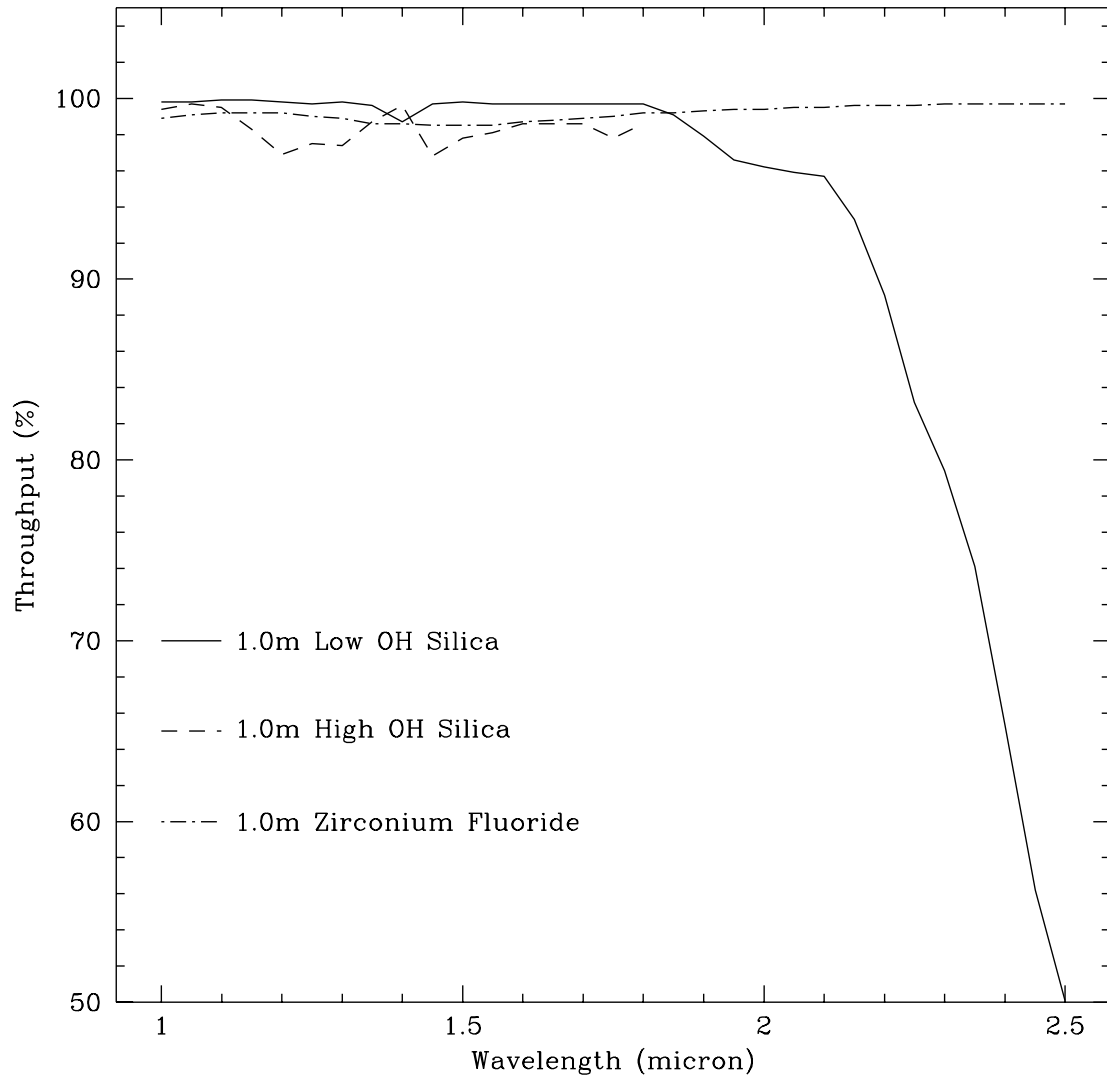


Fig. 3.— Transmission of different types of fiber at infrared wavelengths for 1m lengths.

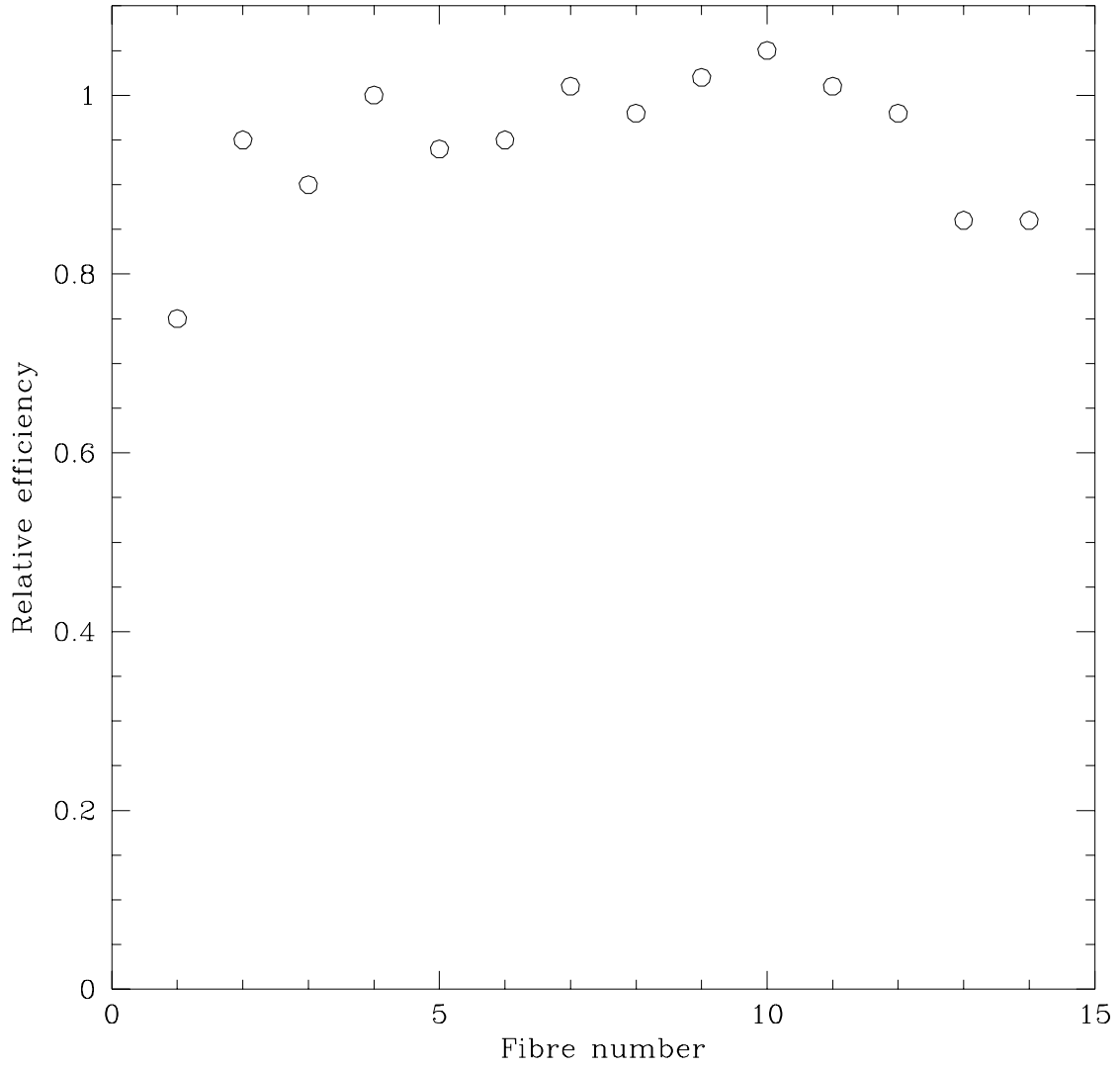


Fig. 4.— Example of fiber to fiber variations in throughput in the MOS mode.

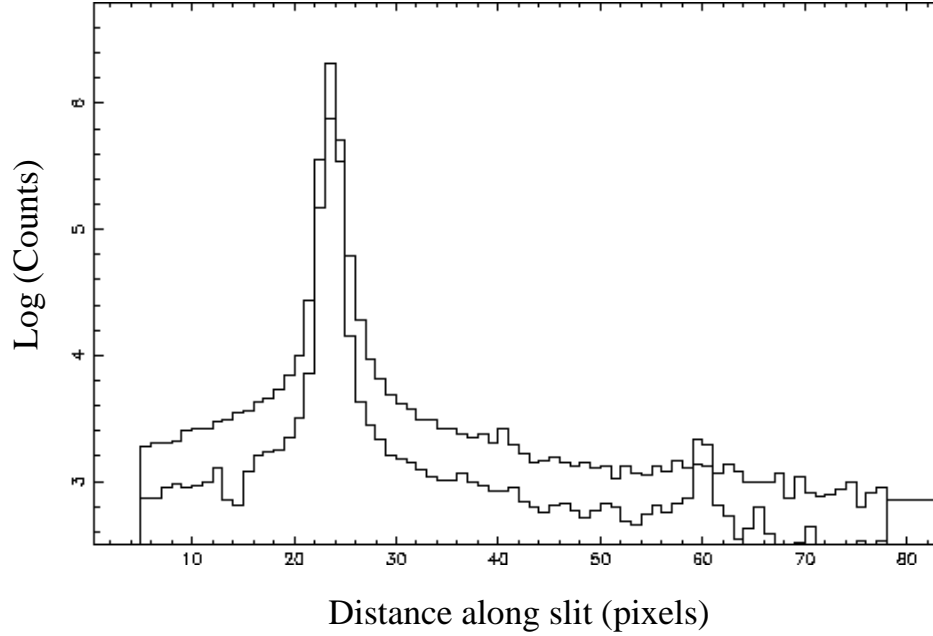


Fig. 5.— Comparison of the spatial profile of a standard star observed with one fiber of the MOS mode (lower trace) and by CGS4 alone (upper trace) on a logarithmic scale of intensity. Note that another object has been caught serendipitously by one of the other fibers.

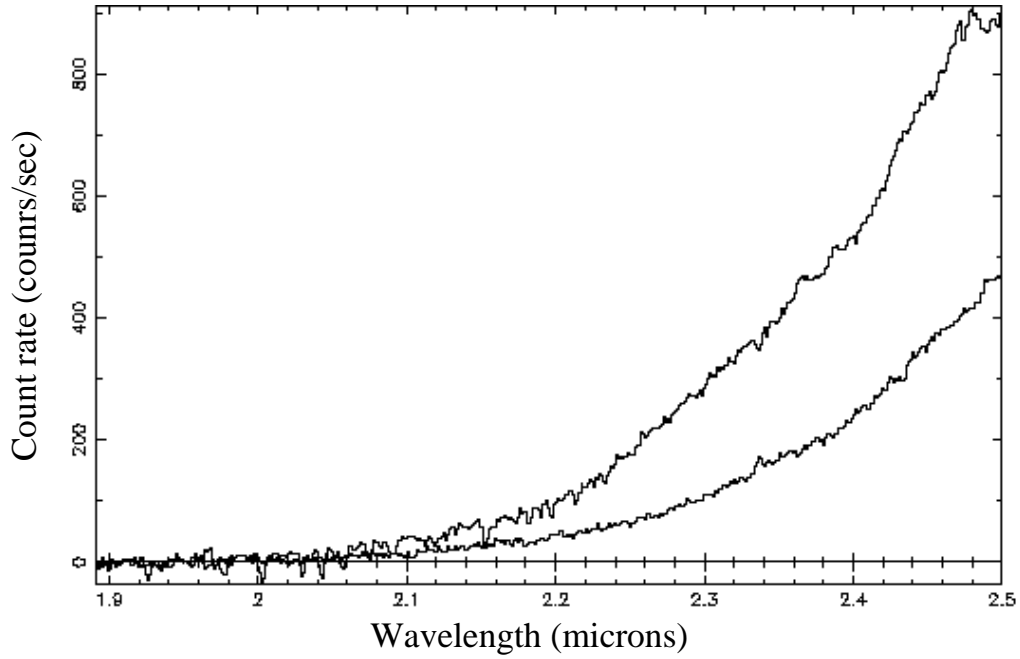


Fig. 6.— Background count rate in the K-band for the MOS mode with the output mask installed for locations within the slit corresponding to the positions of fibers (upper trace) and between fibers (lower trace).

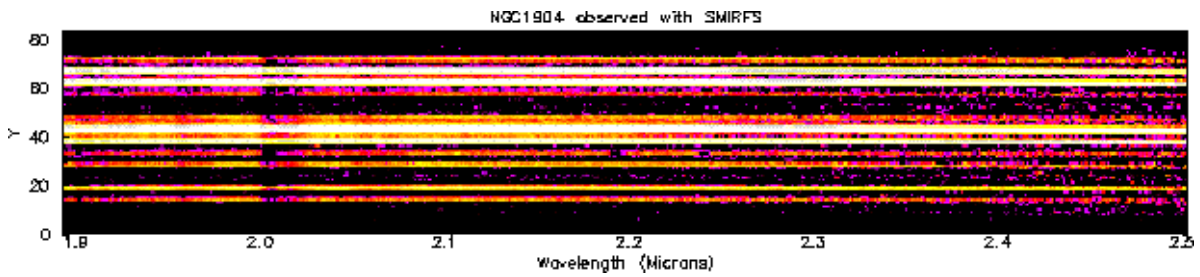


Fig. 7.— MOS-mode background-subtracted spectrogram for NGC1904. This is a subset of the full detector surface.

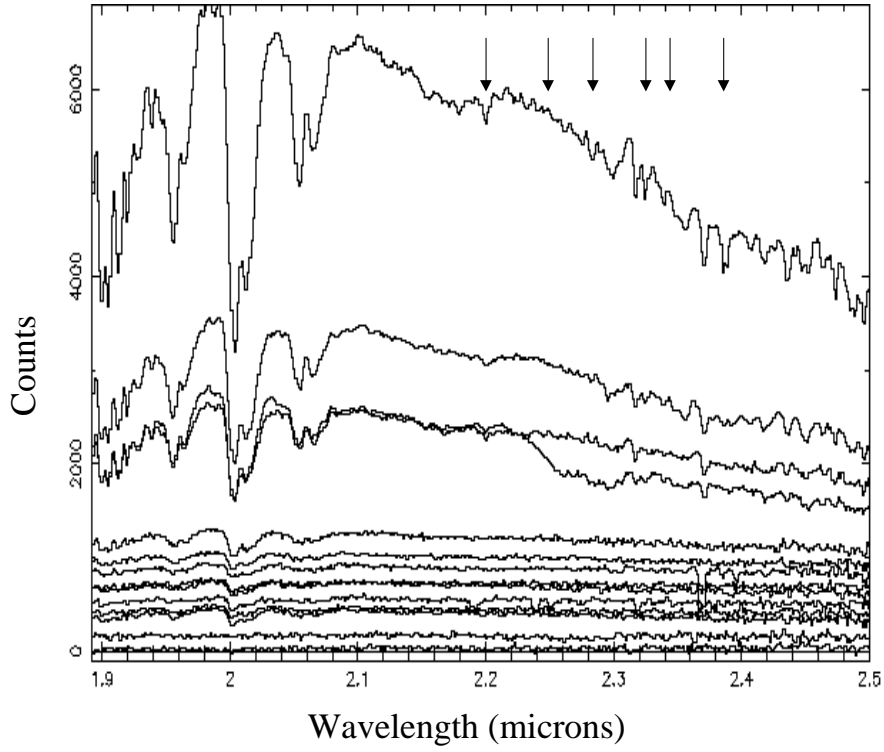


Fig. 8.— Extracted spectra for the NGC1904 observation (Fig. 7). The spectra are offset from each other by 100 counts for clarity. Arrows mark the location of the NaI and CaI lines mentioned in the text and some (12)CO lines.

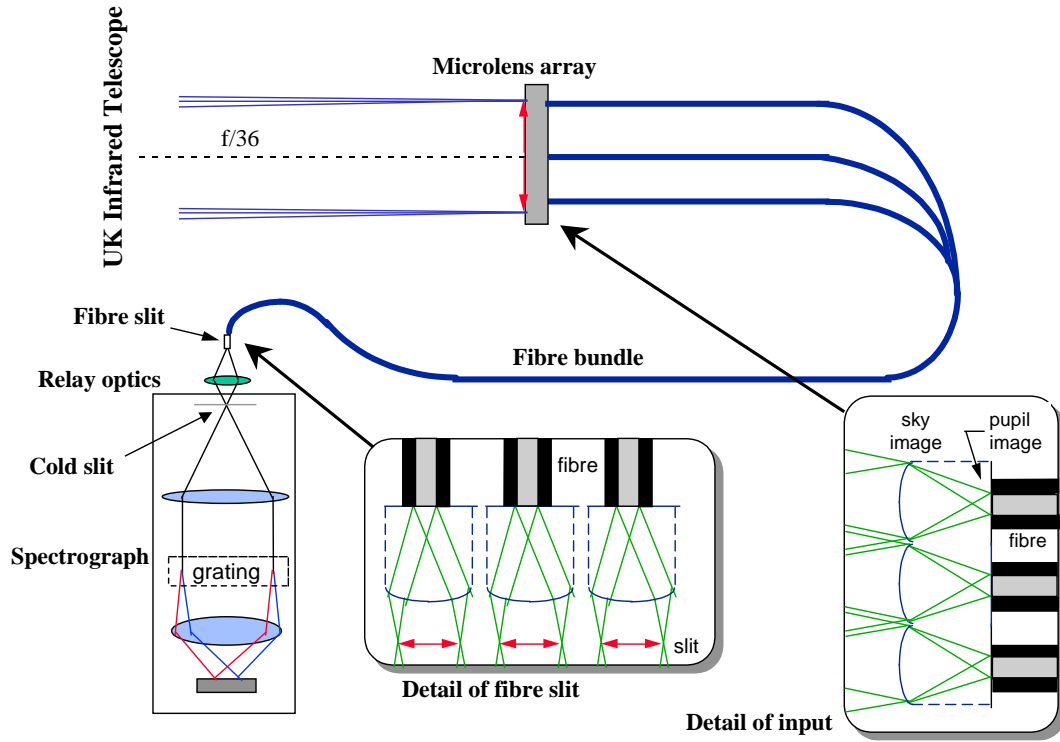


Fig. 9.— Basic principle of the integral field unit (IFU).

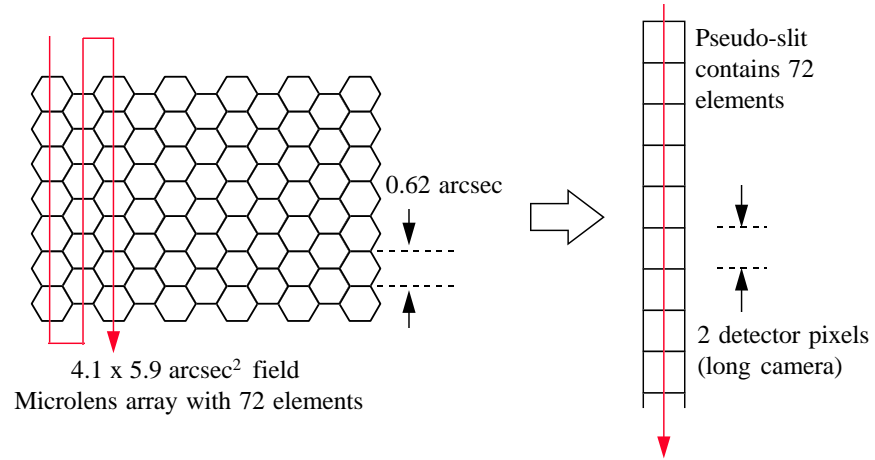


Fig. 10.— The field format of the IFU showing how the elements are reformatted to form the pseudo-slit.

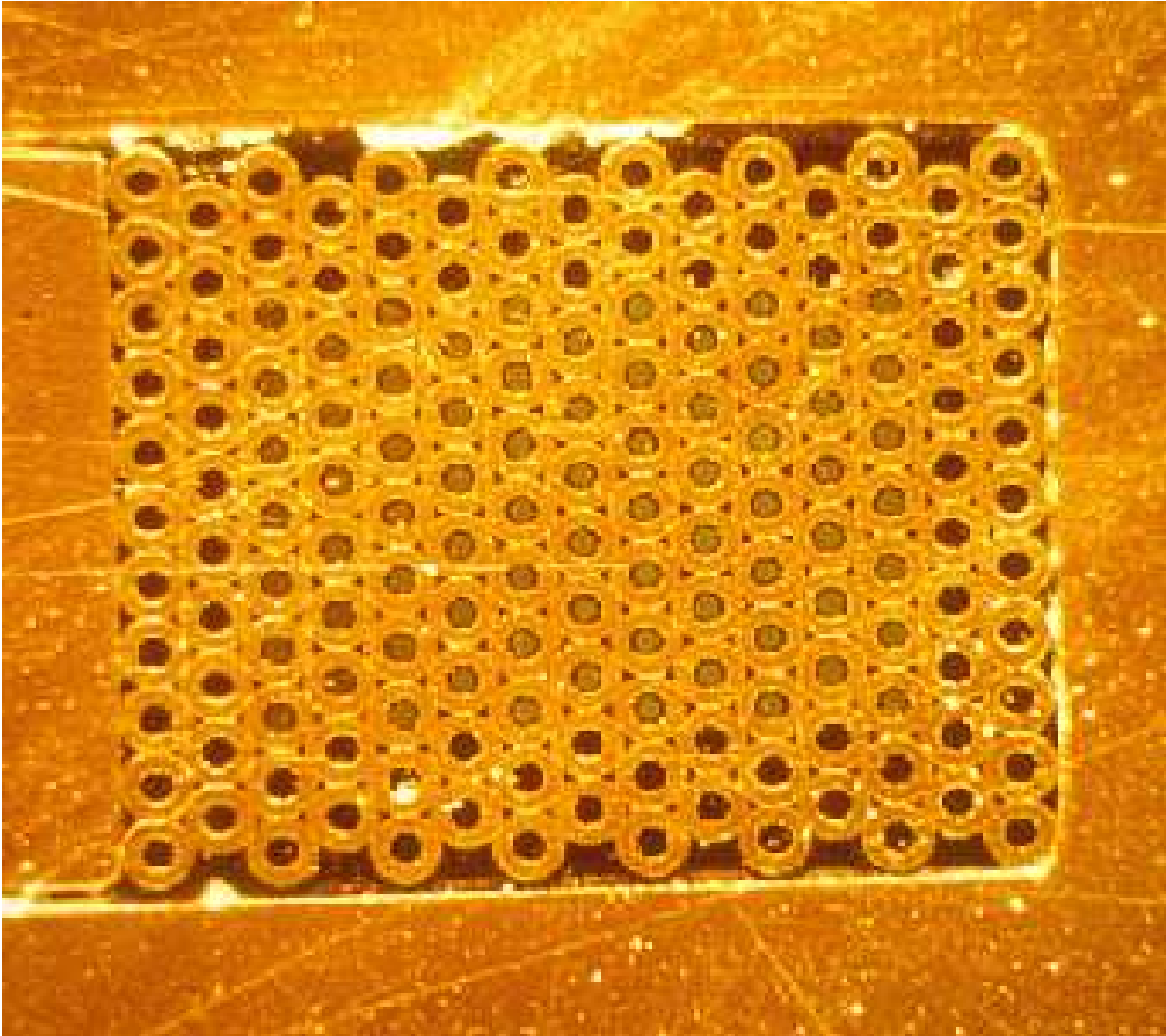


Fig. 11.— The IFU input fiber holder. The fibers are located inside the microtubes. Some microtubes at the edge of the array are not populated. The assembly is shown after polishing but prior to the attachment of the lenslet array. A few large-scale scratches can be seen where a contaminant has been accidentally introduced into the polishing medium but these mostly miss the fibers and do not affect the performance on the system.

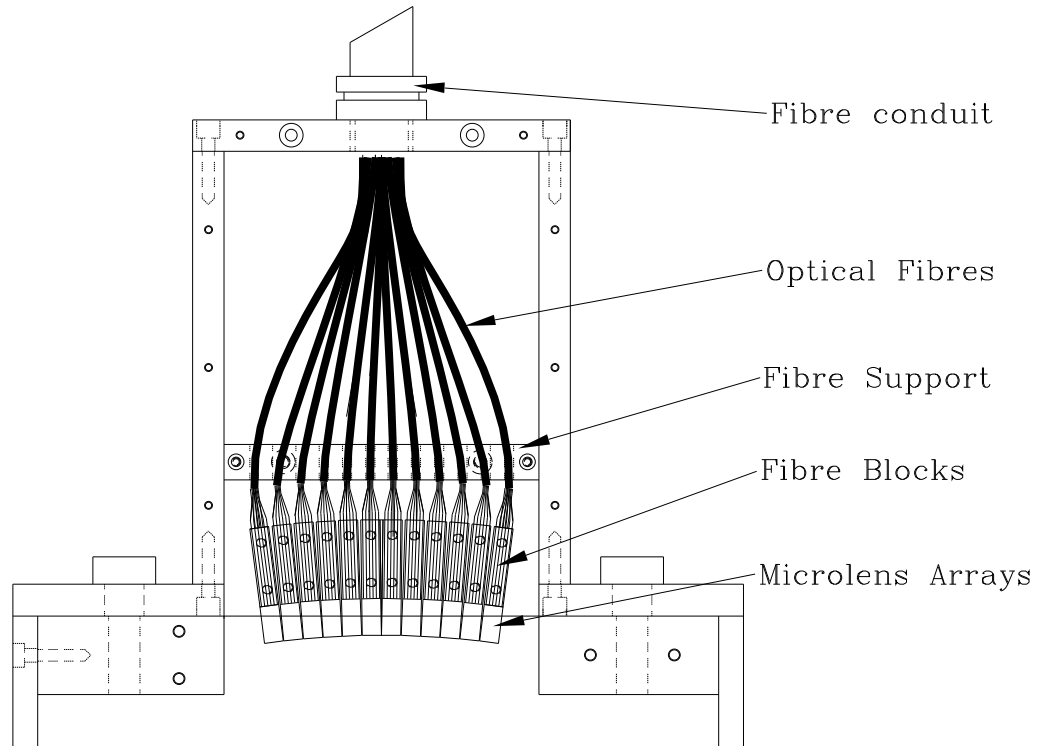


Fig. 12.— The IFU pseudo-slit. This shows how the fibers are arranged at the slit and attach to the lenslet arrays. The curvature of the slit is required to match the spectrograph pupil.



Fig. 13.— Part of the IFU slit assembly showing the polished fibers prior to the attachment of the lenslet arrays.

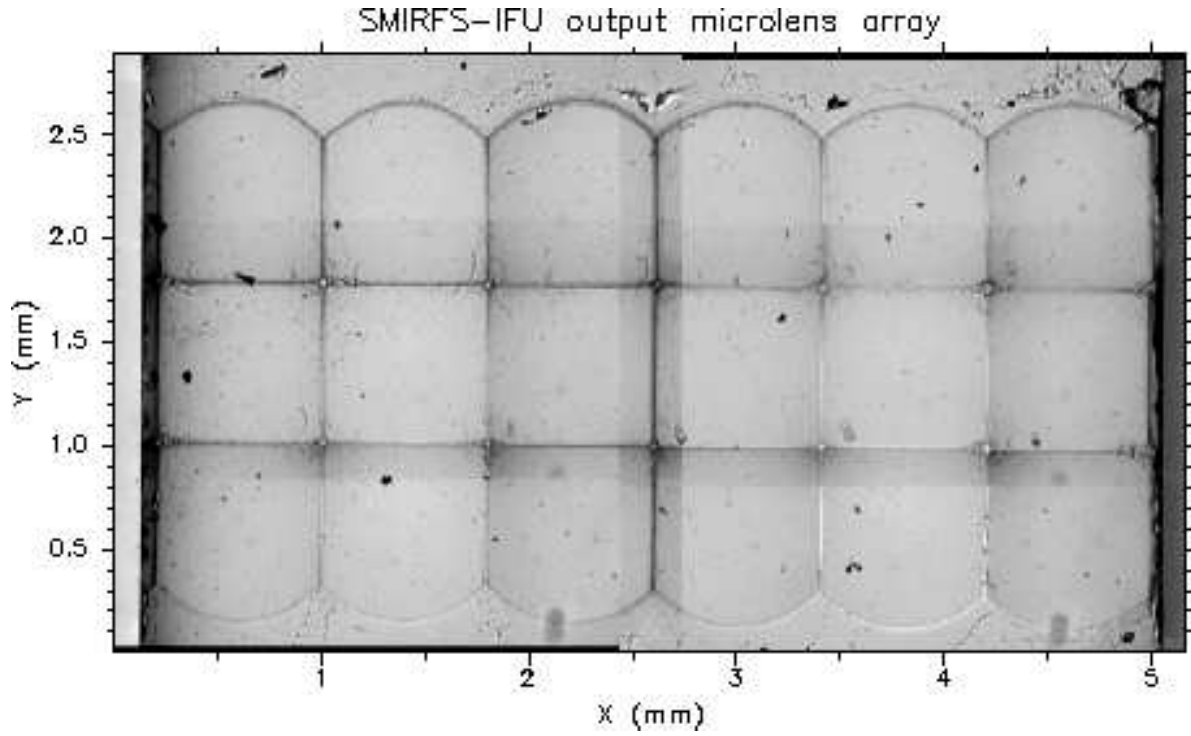


Fig. 14.— One IFU output lenslet array. The dark regions are defects in the lenslets or dust particles. Only the middle row of 6 is used.

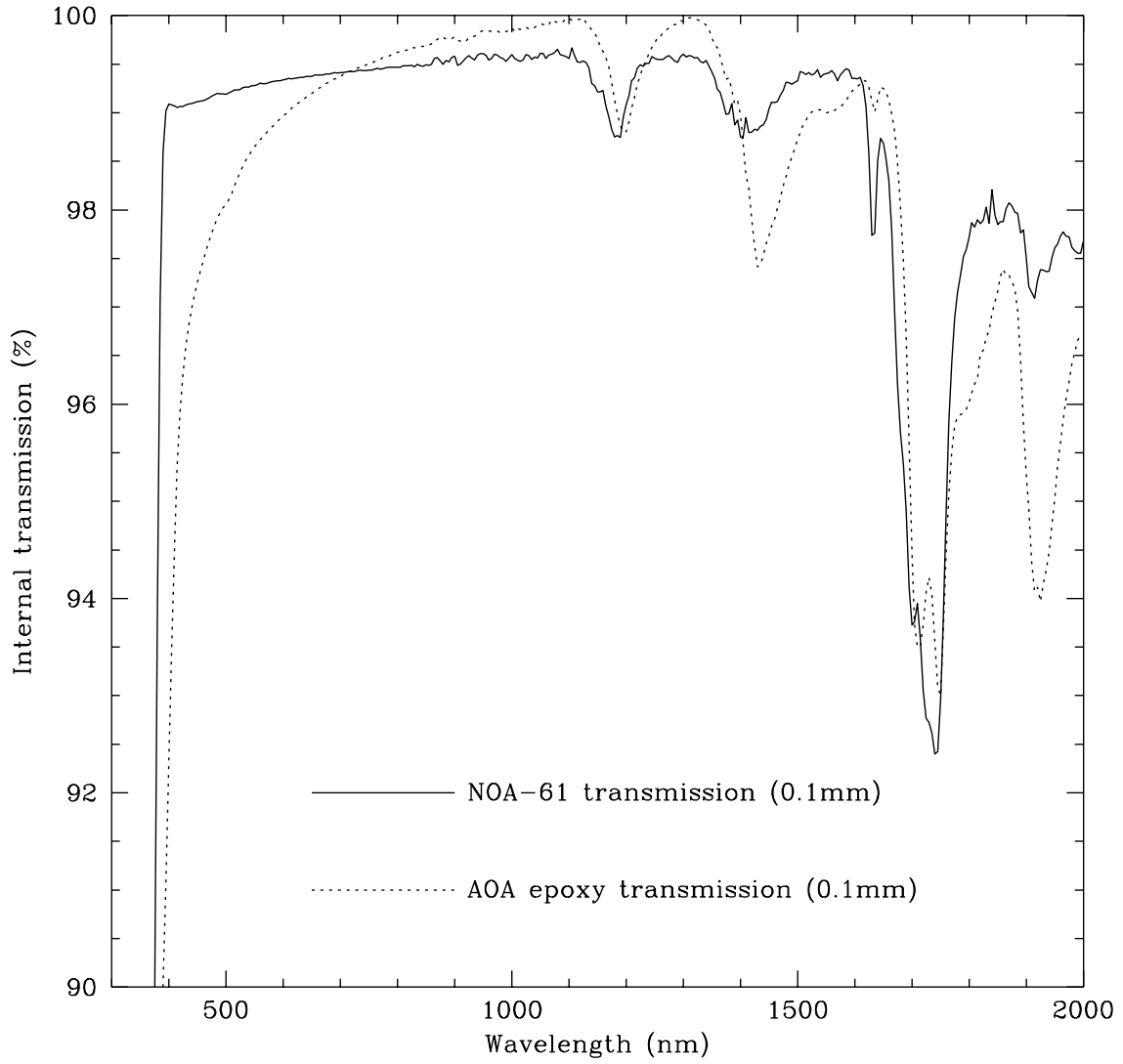


Fig. 15.— Internal transmission of the epoxy used in the IFU lenslet construction and the adhesive used to bond them to the fibers. The data are scaled from our measurements to the typical thickness used in the SMIRFS IFU, as indicated. See Lee (1998) for further details.

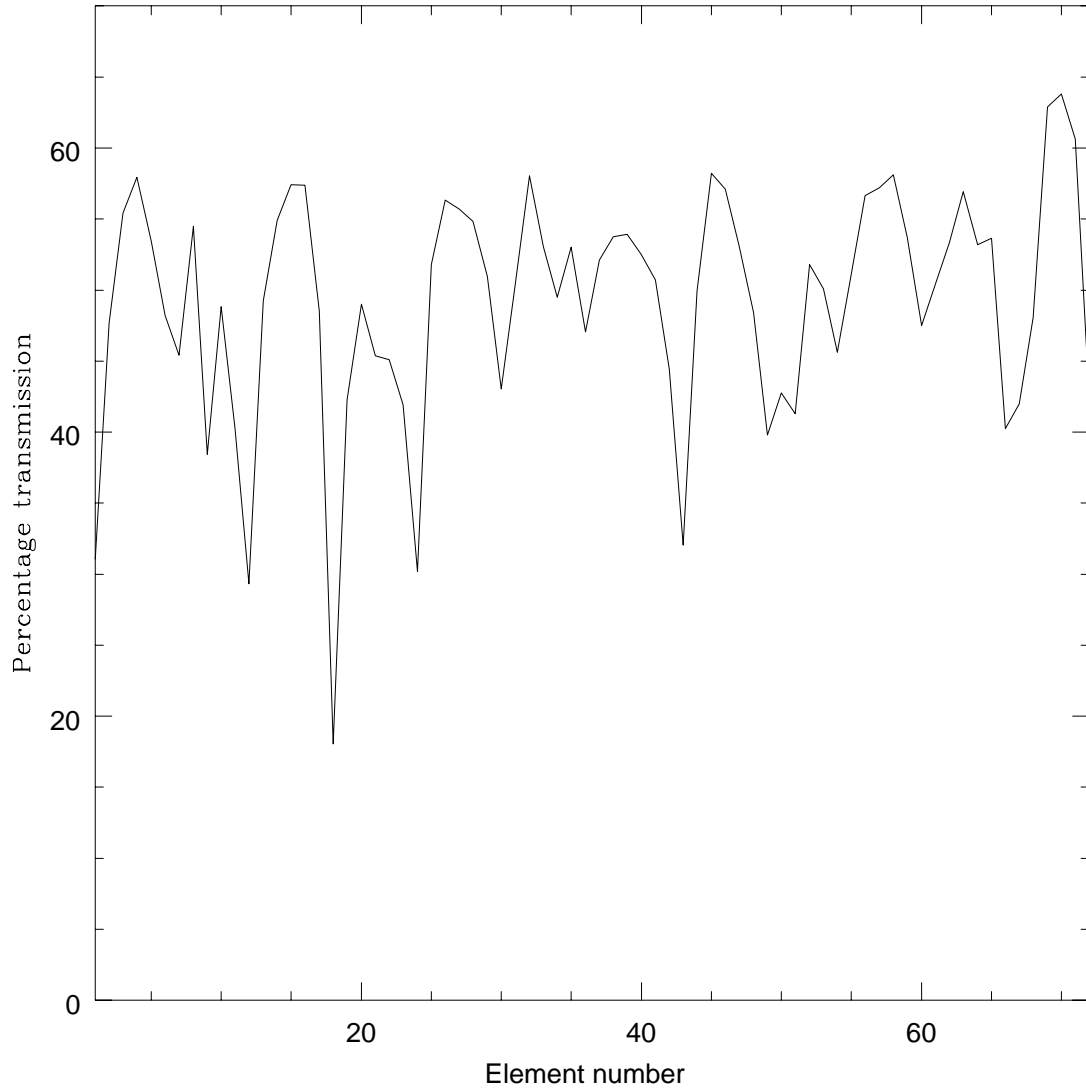


Fig. 16.— Fiber-to-fiber throughput variations for the integral field mode showing the intensity of light recorded along the slit for uniform incident radiation integrated over wavelength. Element 18 has a broken fiber. For elements 12, 24 and 32, the fibers became partially unbonded from the slit during polishing.

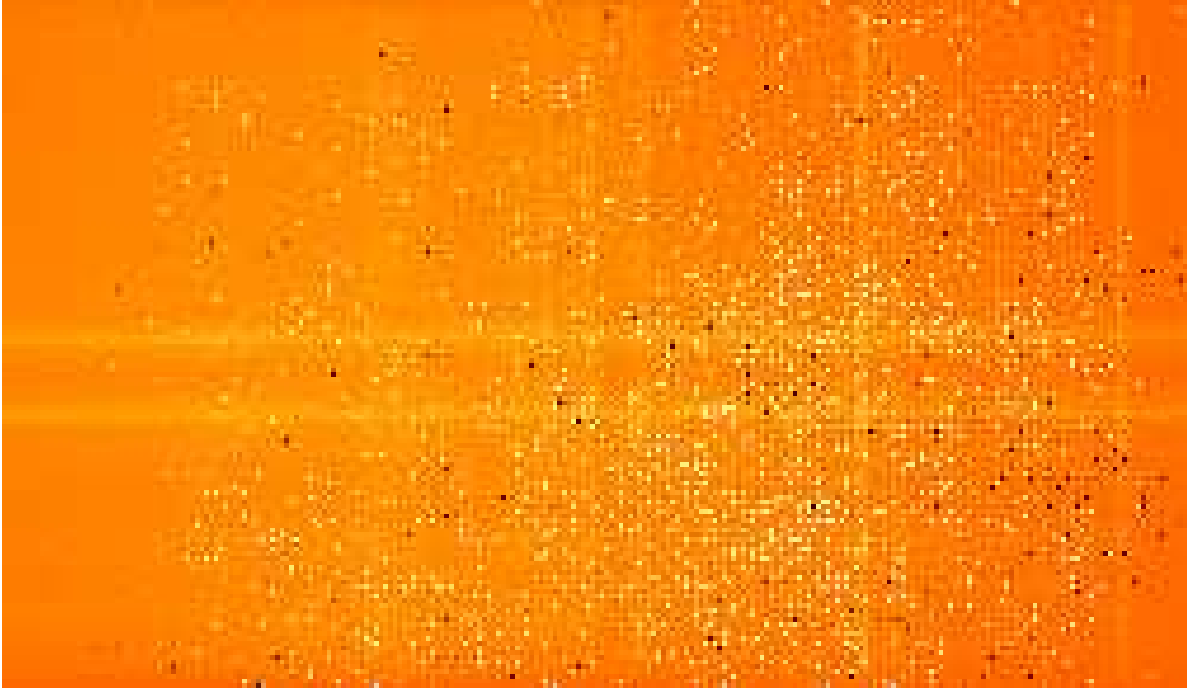


Fig. 17.— An example of a raw integration from CGS4. Wavelength increases from left to right.

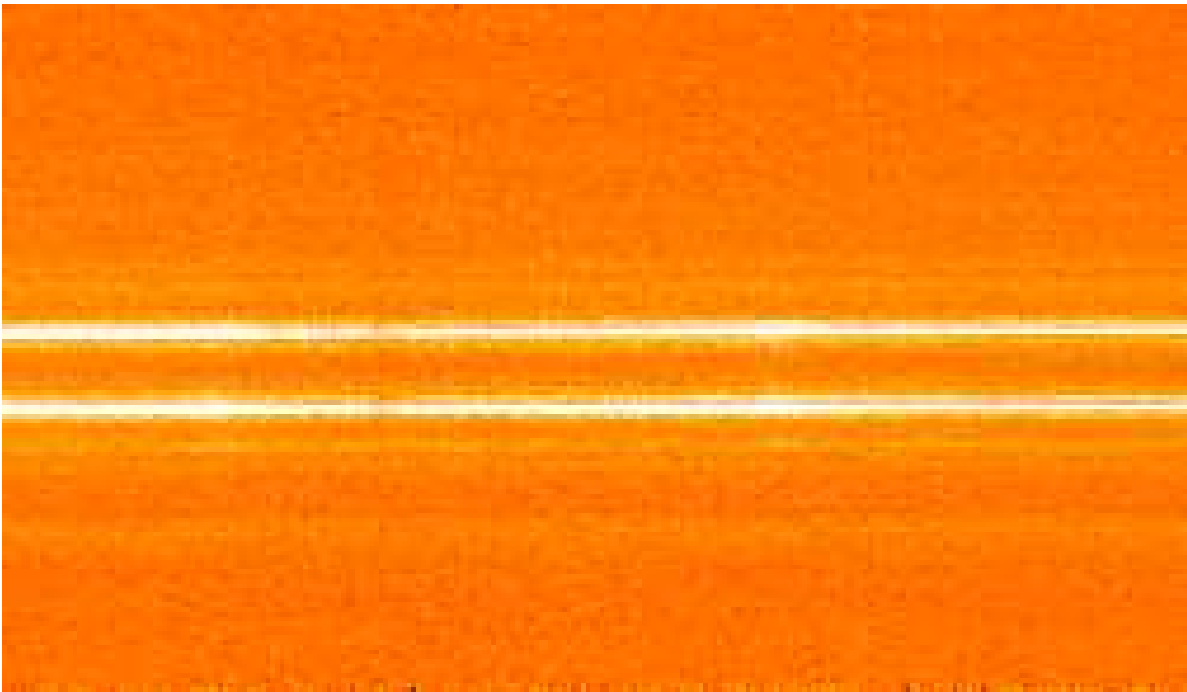


Fig. 18.— An example of a single observation after sky subtracting, flat fielding and combining integrations. Wavelength increases from left to right.

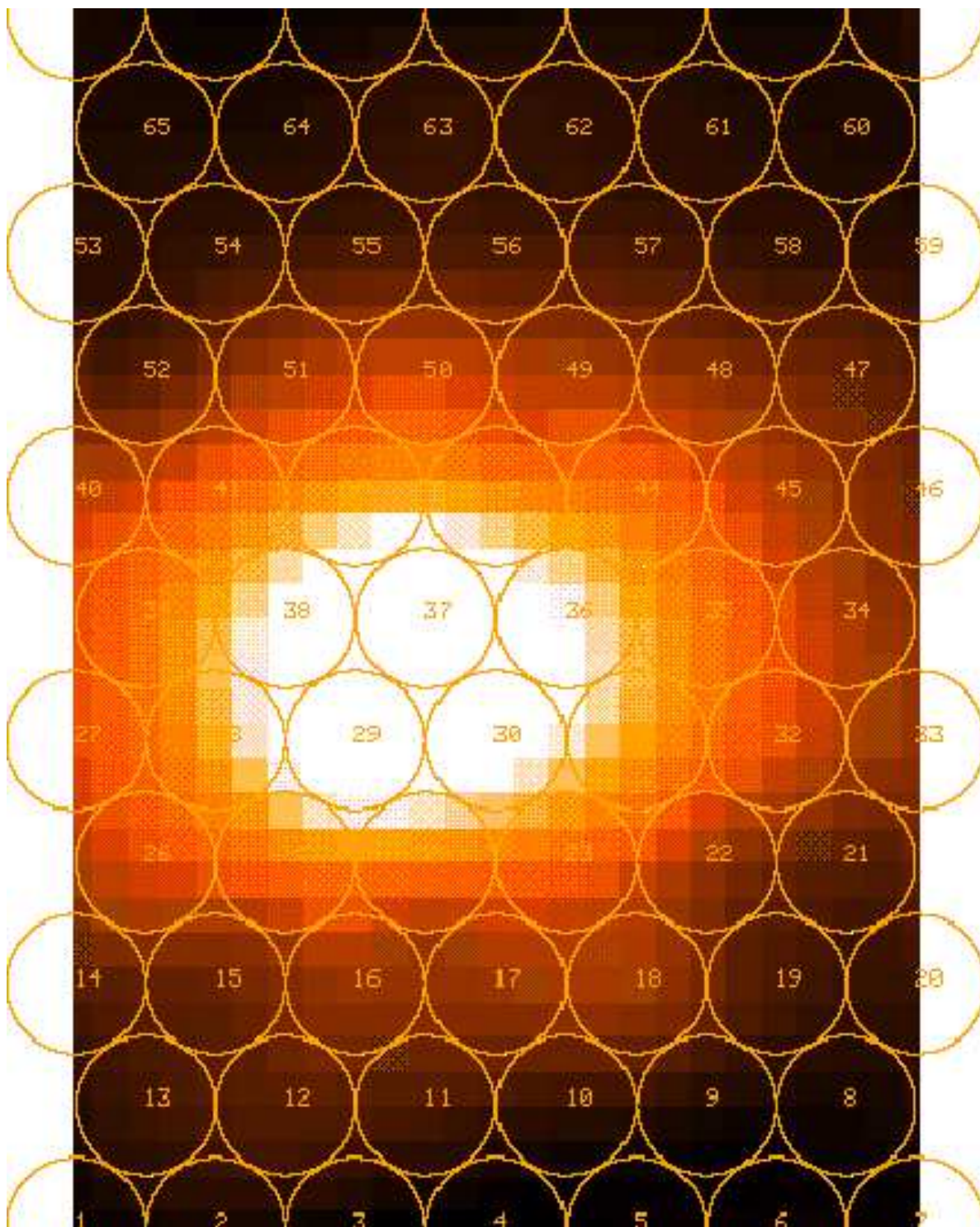


Fig. 19.— An example of a single datacube collapsed in wavelength, with numbered microlens positions overlaid as circles

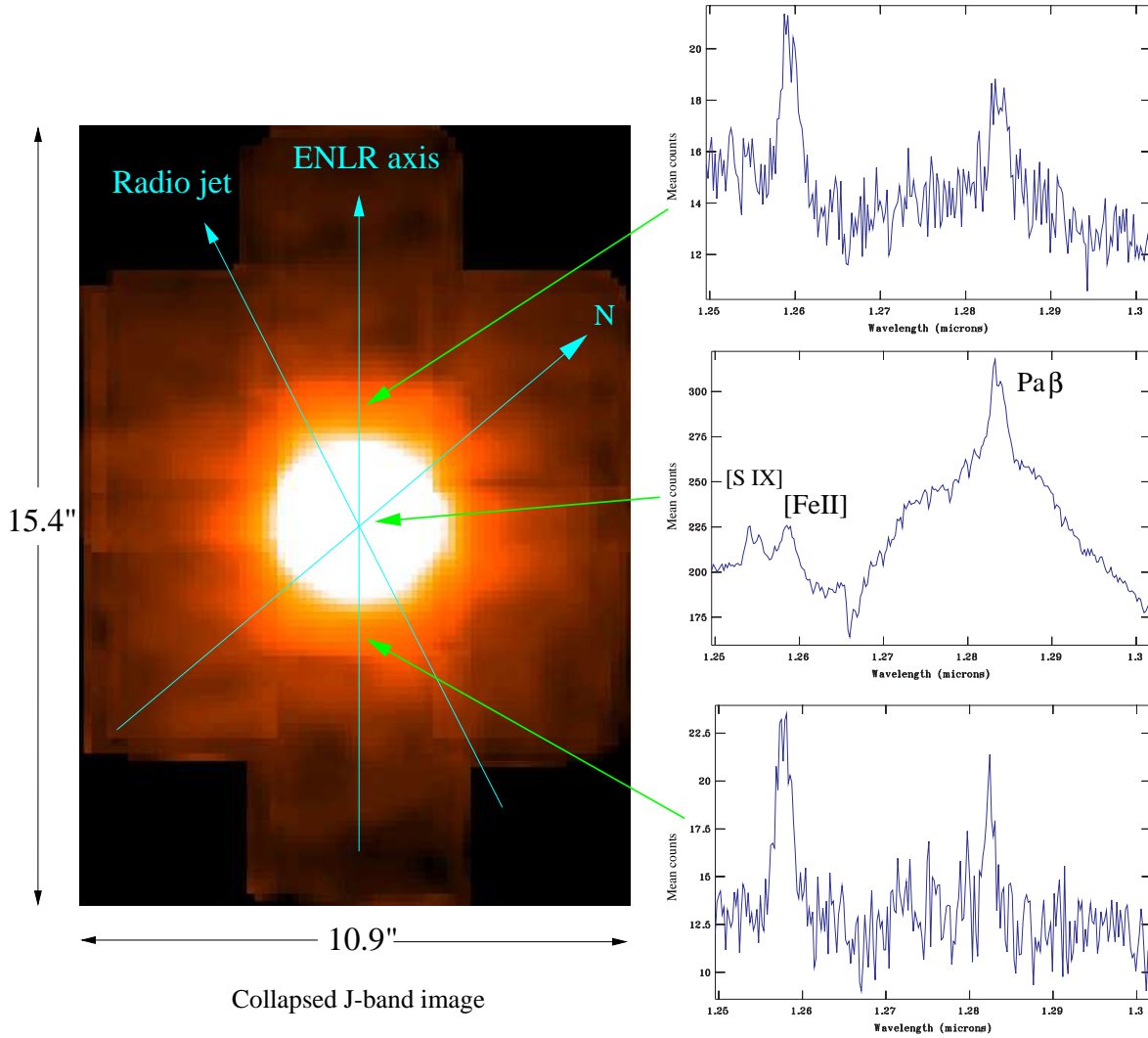


Fig. 20.— Mosaiced integral field mode observations of NGC4151. The image is a white-light reconstruction from the J-band observations. The axes of extended narrow line emission seen at visible wavelengths and the axis of the radio structure are marked. Examples of spectra along selected lines of sight are shown. East is left of North.

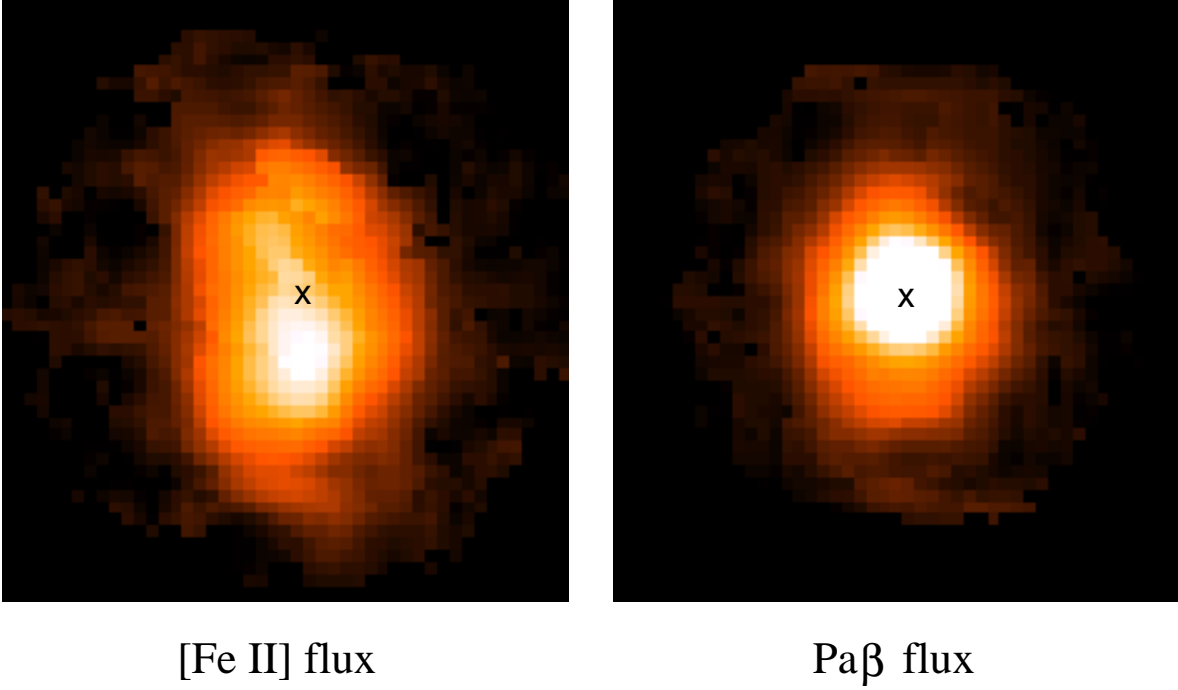


Fig. 21.— Continuum-subtracted image of [FeII] emission and the narrow components of the Pa β emission. Each map covers the central 8×6 arcsec region shown in Fig. 20. The nucleus is marked by a cross.